Zeng, L., Chime, A. C., Chakaroun, M., Ben Smida, S., Nkwawo, H., Boudrioua, A., & Fischer, A. P. A. (2017). Electrical and optical impulse response of High Speed Micro-OLEDs under ultra-short pulse excitation. IEEE Transactions on Electron Devices, 64(7), 2942-2948. DOI: 10.1109/TED.2017.2706723

TED-2016-12-2030-R

Electrical and Optical Impulse Response of High Speed Micro-OLEDs under Ultra-Short Pulse Excitation

L. Zeng, A. C. Chime, M. Chakaroun, S. Bensmida, H. Nkwawo, A. Boudrioua, and A. P. A. Fischer.

Abstract—The electric and optical impulse response of two types of High Speed OLED (HSOLED) driven by ultra-short electrical pulses is investigated. The two HSOLED were designed and manufactured to be characterized in the presence of electrical pulses ranging from 10ns to 100ns in duration and a repetition rate of 10Hz. The impact of the OLED geometry and the fabrication process on the time response is investigated. This is the first time that an optimized HSOLED exhibits an electrical time response as low as 2.1±0.6 ns and also shorter than the device optical decay time (9.8±0.2ns). Moreover, the HSOLED measured current density reaches 3.0 kA/cm^2, the highest value reported in the literature, with state-of-the-art electroluminescence of 12W/cm^2.

***Index Terms*—OLED, pulse excitation of OLED, high-speed OLED.**

I. Introduction

Classically, Organic Light Emitting Diodes (OLED) have been developed for applications such as solid-state lighting [1,2], and displays [3,4]. More recently, new organic optoelectronic devices with high-speed features have been considered as a potential technology to pave the way towards new applications like LiFi [5], photonic above IC [6], backplane transmission [15], and last-mile telecommunications [7]. Moreover, achieving lasing in organic hetero-structures would have also a significant impact on transmission based applications. In particular, high speed coherent organic light source have the potential to become a possible solution for backhaul connections. With their low cost and fast time-to-market, high-speed optoelectronic organic devices can become a candidate technology for the backhaul of femto-cell base stations used in future networks [8]. All the applications quoted above require OLEDs to operate in a high-speed manner.

This manuscript was submitted on December 2016.

This work was supported by the Labex SEAM (Science and Engineering for Advanced Materials), the University of Paris 13, and the University of Bristol.

L. Zeng, A. C. Chime, M. Chakaroun, H. Nkwawo, A. Boudrioua, and A. P. A. Fischer are with Université Sorbonne Paris Cité, Université Paris 13, Laboratoire de Physique des Lasers, UMR CNRS 7538, 99 avenue JB. Clément, 93430 Villetaneuse, France.

A.P.A. Fischer is also with Université Sorbonne Paris Cité, Université Paris 13, Centrale de Proximité en Nanotechnologies de Paris Nord, 99 avenue JB. Clément, 93430 Villetaneuse, France (e-mail : fischer@iutv.univ-paris13.fr)

A. C. Chime is also with Université de Dschang, Institut Universitaire de Technologie Fotso Victor de Bandjoun, BP 134 Bandjoun, Cameroun.

S. Bensmida, is with Communication Systems and Networks Group, Electrical and Electronic Engineering Department, Merchant Venturers School of Engineering, University of Bristol, woodland road, BS8 1UB, Bristol, UK.

High-speed organic light emitting sources is a requirement to achieve high-current densities and high density of excitation in organic hetero-structures which is a prerequisite to lasing. Lasing under electrical pumping in organic semiconductors has not been demonstrated yet. Among a variety of reasons, the excitation density reported in the literature so far does not exceed laser threshold [9]. Recently, several studies reported the electrical and optical response of OLEDs when driven by a pulse in order to achieve high current densities, and hence a step closer to lasing [10-12].

To bridge the gap between current state-of-the-art OLEDs and the discussed applications, devices with high-speed and high-current density characteristics are required. Therefore, this work investigates the feasibility of high-speed organic optoelectronic devices for new applications. This implies the improvement of the time response of the organic optoelectronic devices which is due to their resistive and capacitive equivalent elements (and their associated RC product). A modelling approach was followed to study the impact of the fabrication process and geometry of two OLEDs on their electrical and optical responses. More precisely, this study focuses on how the geometry and the fabrication process impact the OLED impulse response by straightforward analysis of a modified electrical model [13][14] that takes into account the on-off regime, in the presence of an ultra-short pulse. This leads to identify and optimize the dominant parameters/elements that limit the time response of the OLED. This is achieved by relating/linking these dominant model parameters into physical parameters, and useful guidelines for the fabrication of OLEDs were then deduced and formulated.

Two OLEDs based on different processes have been fabricated. Each OLED is then characterized experimentally in terms of its electrical and optical response. The main goal is to achieve fast and high voltage pulse excitation of the OLED to reach high current densities while avoiding the device failure; In general, high-speed/ultra-short pulsed excitation with low repetition rates prevents thermal failure resulting from high-current density. This paper is structured as follows; In the section II, the electrical model of the OLED is explained to identify the parameters that affect the electrical impulse response. In section III the fabrication process of the two characterized OLED is explained, whereas the characterization setup and results are described and discussed in section IV. Finally, the conclusion lays down some design considerations for future work.

II. EQUIVALENT ELECTRIC CIRCUIT

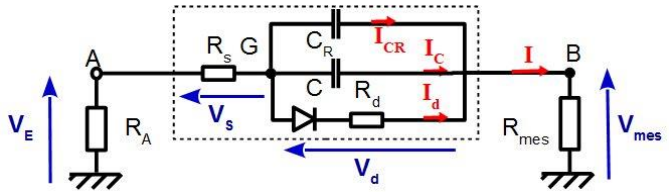

Fig. 2. Equivalent electrical circuit for pulse excitation in ON-OFF configuration. R_S, serial resistance taking into account the electrode geometry, R_D diode resistance, C junction capacitance, C_R process dependent fabrication

In terms of input/output behavior, the OLED response can be discomposed into an electrical transfer function and an optical one. The electrical transfer function relates he excitation voltage as an input to the current density as an output while the optical transfer function relates the exciton density (via the current density) as an input to the electroluminescence (or the photon emission) as an output. In the current section authors focus mainly on the electrical response. The approach consists of a numerical study of an existing OLED electrical model modified to take into account the on-off configuration [13][14]. The goal is to identify which parameter/element of the model affects the most the electrical impulse responses. In On-Off configuration, the OLED equivalent circuit is modeled with a resistance R_S taking into account the electrodes geometry, with an ideal diode in series with a resistance R_D, with a capacitance C in parallel, and eventually, with another capacitance C_R as shown in Fig.1. The capacitance C takes into account the junction capacitance while C_R models the parasitic capacitance resulting from the fabrication process used to define the OLED active area. V_{MES} is the voltage across the resistor R_{MES} and $V_E(t)$ is the excitation voltage. Simulation results of this equivalent model in the presence of a pulse excitation are shown in Fig. 2. For a pulse excitation with amplitude A, the voltage across R_{MES} exhibits a sharp rise reaching a peak current value I_{PEAK} followed by an exponential decay to a steady state current value I_{ST} as shown in Fig.2. The current I flowing through R_{MES} is the sum of I_D, I_C, and I_{CR}, which are the currents flowing through the diode and R_D, the junction capacitor C, and the fabrication process capacitor C_R, respectively. The currents I_C and I_{CR} appear during the transient regime then vanish after the decay time τ (95% decay after 3τ); This results in $V_{MES}(t) = V_{ST} = R_{MES} \times I(t) = R_{MES} \times I_D(t)$, which provide a mean of assessing the current density $J(t)=I_D(t)/S$ once the steady state is established (where S is the considered OLED active surface). Therefore, the relevant current flowing through the OLED must be measured once the steady state is established after three times the time response (3τ). In other words, the capacitances are charged first which produces the peak current I_{PEAK} followed by a decay in current that allow the current through the active part of the OLED to flows progressively. If the pulse width is too short and ends before

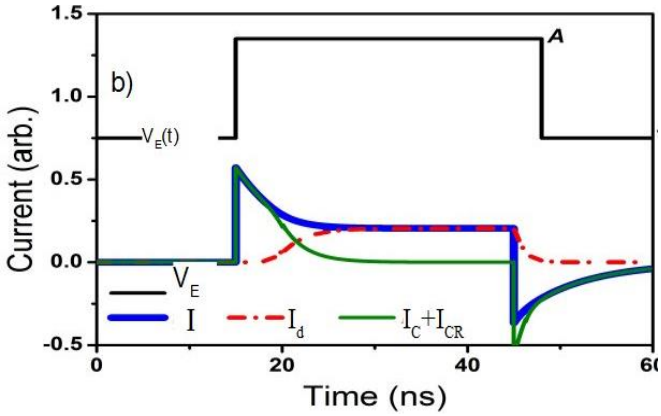

Fig. 1. Numerical study of the Electrical Impulse response of the µ-OLED calculated with C=50pF, R_S=45Ω R_D=100Ω,.Threshold voltage of the diode is 40V. Upper trace is the excitation voltage. Lower trace: Thin green continuous line is the capacitance current I_C, red dotted line is the current through the diode and R_D, I_D, and thick blue line is the current I_{MES}.

the capacitance current vanishes, the current flowing through the organic diode remains negligible and the latter hardly lights-up. Therefore, there is a minimum pulse duration for an OLED to operate efficiently with significant light emission because of the transient regime described above. In order to be able to excite an OLED with an ultra-short pulse and to reduce the transient regime duration, the time response τ of the OLED has to be minimized. The key parameters to reduce the time constant τ are (R_S+R_{MES}), R_D, C and C_R; R_{MES} is dictated by the measurement setup; as the signals in use are in the RF domain and to avoid reflection R_{MES} is chosen to be 50 Ω. The anode resistance R_S depends on the fabrication process. Therefore, the decrease of both the serial resistance R_S and of the measurement resistance R_{MES} is limited. However, the decrease of R_D can be addressed either by the optimization of the organic hetero-structure to reduce the OLED threshold voltage or by the increase of the operating point via the increase of the amplitude A of the excitation voltage. Both considerations are out of the scope of this paper which focuses on the influence of the fabrication process on the time response and on the capacitances that appear as dominant. In the next section, we investigate experimentally how to control this critical capacitance value during the fabrication process, to optimize the time response.

III. DEVICE FABRICATION

The impact of fabrication geometry of the micro-OLED (µ-OLED) and hence the capacitances is investigated in this section. The processes developed and compared in this study are the following; in the first process, the size of the µ-OLED is delimited by an insulating photo-resist, while in the second process the µ-OLED is defined by electrode crossing.

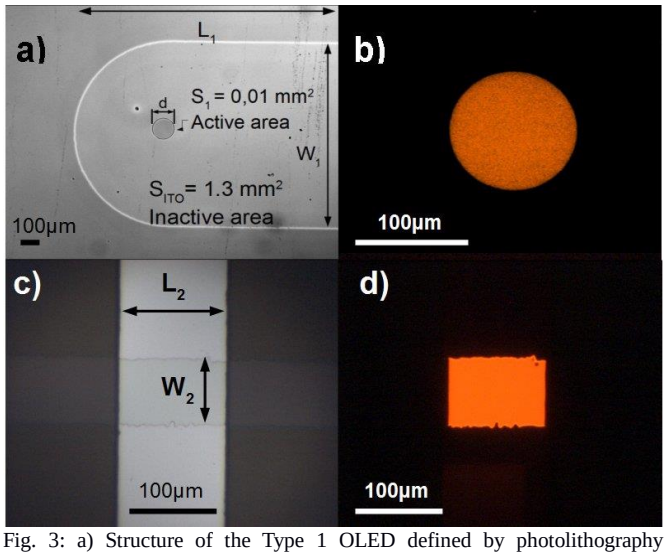

Fig. 3: a) Structure of the Type 1 OLED defined by photolithography observed with a 2× optical zoom before the aluminum cathode deposition: The central dark grey circular surface correspond to the active area (diameter d=113µm, S_1= 0.01mm^2) surrounded by insulating photoresist in light grey (Inactive area S_{ITO}= 1.3mm^2+-0.01mm^2). The ITO stripe (not entirely visible) is L_1=3 mm long and W_1=3 mm width. b) OLED1 in the ON state with 1 mA DC current observed with a 20× optical zoom. c) Structure of the OLED2 defined by electrode crossing observed with a 10× optical zoom. The ITO stripe width is W_2=87µm, the aluminum cathode width is L_2= 120µm width. Active area is S_2=0,01mm^2 d) OLED2 in the ON-state with light emission with 1mA DC current observed with a 10× optical zoom.

A. Type 1 process: photoresist delimited µ-OLED (OLED1)

The first process consists of the following steps; the planar ITO anode is etched to form a 3 mm long, 1 mm-wide stripe resulting in a serial resistance R_{S1}=45Ω. A t_R=200nm thick photoresist is then deposited by spin-coating, and irradiated by photolithography in order to free a round shaped hole of ITO that defines the active area S_1=0,01 mm^2 (Fig.3.a). The organic hetero-structure of the OLED and the metallic cathode are then deposited on the substrate by thermal evaporation covering an area larger than the ITO anode. The organic hetero-structure studied in this work is: m-MTDATA (4,4',4"-Tris[(3-methylphenyl) phenylamino] triphenylamine) (30 nm) / NPD (N, N′-Di(1-naphthyl) – N, N′- diphenyl – (1,1′-biphenyl) -4,4′- diamine) (10 nm) / Alq3 doped with 2% of DCMII (aluminium tris-(8-hydroxyquinoline) doped with (4-(dicyanomethylene)-2-methyl-6-julolidyl-9-enyl-4H-pyran) (2% in weight, 30 nm) / BCP (2,9-Dimethyl-4, 7-diphenyl-1, 10-phenan- -throline) (5 nm) /Alq3 (25 nm) /LiF (1 nm) /Al (100 nm) giving a total thickness of the organic layers t = 101nm. In this first process, both the ITO anode stripe width W_1 and the OLED active area are well controlled by the photolithography step with a precision of 1 micrometer which opens the possibility to fabricate a µ-OLED as small as 1µm. It is worth noting that the part of the ITO located around the OLED active area and covered by the insulating photoresist and the organic compounds and ultimately by the aluminium cathode constitutes the parasitic capacitance C_R. The corresponding inactive area is S_{ITO} = 1.3 mm^2.

B. Type 2 process: electrode crossing delimited µ-OLED (OLED2)

The second process is developed to produce an OLED (OLED2) with smaller C and C_R capacitance values. The ITO is etched to form a W_2=87 µm width, 1 mm long stripe. The organic hetero-structure is then deposited directly on top of the substrate on a large area. To limit the OLED size, the cathode is deposited through a special shadow mask with narrow slits (L_2=120µm width). The active area is determined by the superposition of the two perpendicular striped electrodes and hence $S_2 = W_2 \times L_2 = 87 \times 120$ µm^2=0.01mm^2. The cathode mask has to be in contact with the substrate to avoid vapor diffusion which increases the cathode width. To ensure this, the substrate is taken out of the vacuum chamber and aligned with the cathode mask in the glove box filled with nitrogen (1ppm O2). In the current process, the parasitic fabrication capacitance C_R is removed but the narrow ITO anode induces a higher serial resistance R_{S2}=150 Ω. Contrary to the first process, no inactive area susceptible to induce a parasitic capacitance C_R results from the current process, but it does not allow the fabrication of much smaller active areas due to process limitation, therefore, it is difficult to reduce much further L_2 and W_2.

IV. Characterization

The characterization setup consists of a high-speed high-voltage excitation electronic circuit driving the µ-OLED, and a high-speed light collection setup. The excitation circuit includes also a matching resistance R_A=50 Ω to protect the pulse generator, and a serial resistance R_{MES} = 50 Ω dedicated to the measurement of the instantaneous current *I* as shown in Fig.1. Devices are driven by a fast pulse generator (AVTech AVL-2A-B) which produces electrical pulses with a width varying from 3 ns to 100 ns, 10 Hz repetition rate and an amplitude up to 160V. The excitation pulses have a rise time of 2 ns. The light collection setup includes a confocal microscope for the observation and the detection is performed via an avalanche photodiode (Thorlabs, APD130A). All signals are acquired with a high-speed oscilloscope (Tektronix, TDS7254).

A. Characterization of device 1 (OLED1)

Firstly, OLED1 is driven with 90 V amplitude pulses and with different pulse durations ranging from 15ns to 100 ns. The current densities J(t) calculated from the measurement of VMES(t) and the time domain electroluminescence (EL) waveforms are plotted Fig.4.a and 4.b, respectively. During the transient mode, typical current waveforms exhibit an overshoot at IPEAK = 3.65 kA/cm2 which is followed by an exponential decay that declines to a steady state value IST = 1.25 kA/cm2. This is in agreement with the simulation presented in Fig.2 which validates the electrical model. Irrespective of the duration of the pulse, the various responses overlap at the overshoot.

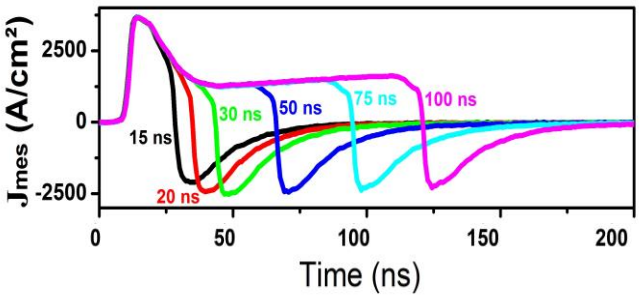

a) Current density as a function of time. Decay time from the overshoot to the steady state plateau is 2=0.9ns.

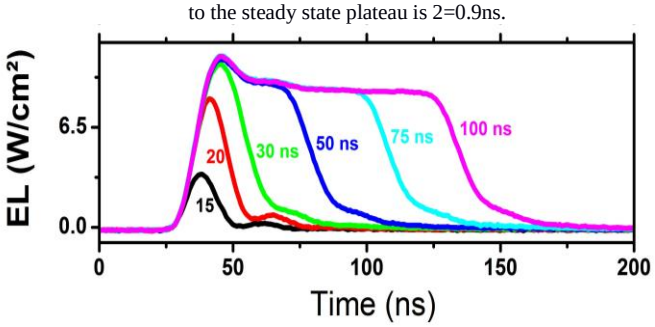

b) Electroluminescence as a function of time: EL decay from the overshoot to a steady state value with a decay time of 25ns.

Fig. 4: Electric and optical response of OLED1 defined by photolithography (S_1=0.01mm2) for 90 V excitation and 3ns, 10ns, 30ns 40ns and 50ns pulse durations.

For pulse durations above 30ns, the OLED electrical responses converge to the same value which defines a plateau corresponding to the steady state current I_{ST}. For this reason, the current density can be estimated from the "plateau" only for pulse durations longer than 30 ns. From the decay-time in Fig. 4.a the electric time constant of OLED1 is estimated to be τ_{1E} = 9.6 ± 3.3 ns. From Fig.4.b, the 50 ns, 75 ns and 100 ns duration waveforms show EL overshoot before a steady state is reached. However, the EL peak is not reached with 15 ns and 20 ns pulse duration. The maximum of EL is also reached for the 30 ns duration pulse but the EL steady state is not achieved, therefore the 30 ns constitute the limit for an efficient and observable step response of the OLED1. The optical time constant is measured to be τ_{1O} = 12.1 ns ± 0.5 ns.

B. *Characterization of device 2 (OLED2)*

OLED2 is driven with 90 V amplitude pulses and with different pulse durations ranging from 3 ns to 50 ns. Current waveforms and EL responses measured for OLED2 are shown in fig.5.a and 5.b, respectively. Current density waveforms exhibit a sharper overshoot, in comparison to OLED1, at I_{PEAK} = 1 kA/cm^2 followed by a decay to a steady state I_{ST} = 0.5 kA/cm^2.

In Fig 5.b, only for pulse durations larger than 10 ns, the EL exhibit overshoots reaching the same maximum value above 6 W/cm^2. This indicates that for pulse durations smaller than 10 ns, the OLED2 does not respond efficiently. The exponential decay time of the optical response is measured to

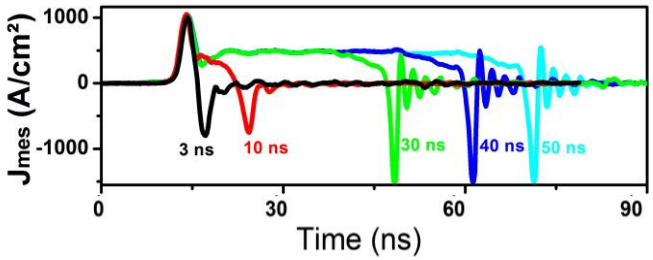

a) Current density as a function of time: Electrical decay time from the overshoot to the steady state plateau is τ_2=0.9ns

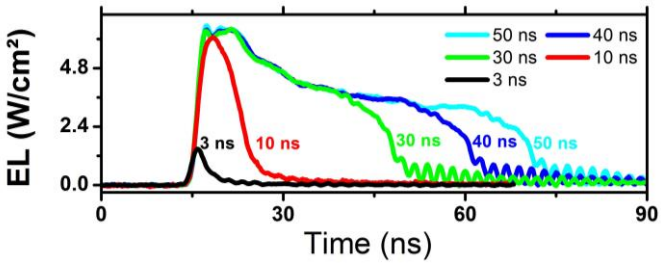

b) Electroluminescence as a function of time. EL decays from the overshoot to a steady state value with a decay time of 25ns.

Fig. 5: Electric and optical response of OLED2 defined by electrode crossing (S_2=87 × 120 µm^2) for 90 V excitation and 3ns, 10ns, 30ns 40ns and 50ns pulse durations.

be τ_{2O} = 9.8 ± 0.2 ns.

V. ANALYSIS

In terms of input/output behaviour the electrical transfer function H(s) and the optical transfer function G(s) composed the OLED total transfer function R(s) = H(s) . G(s). The analysis is therefore divided into the three subsections; firstly, the analysis of the electrical response to a pulsed excitation of H(s), secondly that of the OLED response to a pulsed excitation of R(s) which gives a better insight to the final analysis of the optical response G(s).

A. *Electrical response*

In fig. 4.a and 5.a, the experimental responses to pulsed excitations of the electrical transfer function matches qualitatively the numerical results in fig. 2 and the partial overlap of the waveforms confirms the linear and time invariant nature of the electrical part of the system.

The comparison of the current density decay of OLED1 and OLED2, as well as the electrical time constant ($\tau_{2E} < \tau_{1E}$) demonstrates that the electrical transient regime has been reduced by almost a fivefold factor. Clearly, the fabrication process of OLED2 allows a significant reduction of the electrical time constant resulting from the suppression of the fabrication capacitance C_R that compensates the increase of the serial resistance R_{S2} = 150 Ω (>R_{S1} = 45 Ω). Using the current waveforms and the series resistances R_{S1} = 45 Ω, R_{S2} = 150 Ω and R_{MES} = 50 Ω, the device capacitances can be estimated by numerical fitting as C_1+C_R= 340 pF and C_2=13 pF for OLED1 and OLED2, respectively.

It is worth noting that based on C2, the $C_1 = C_2 S_1/S_2$ capacitance, the surface capacitance of the active area, and ε_{rorg} the averaged relative permittivity of the organic hetero-structure in the nanosecond time scale can be evaluated to $C_1 = 12.7$ pF, 124 nF/cm^2, and $\varepsilon_{rorg} = C_1 t/(S \varepsilon_0) = 12.7$, respectively. These values give access to the parasitic capacitance of the inactive area $C_R = 327$ pF, the corresponding surface capacitance $C_R / S_{ITO} = 25$ nF/cm^2, and the relative dielectric constant of the photoresist $\varepsilon_{rPR} = C_R t_R / S_0 = 5.1$. Note, that OLED1 and OLED2 have almost equal active areas $S_1 \sim S_2$ and thus almost equal capacitances $C_2 \sim C_1$. These values are summarized in table 1.

Table 1 : Resistors and capacitances of the OLED types.

OLED #	R_{si}	C_i	C_R	C total
OLED 1	$R_{S1} = 45\ \Omega$	C1=12.7 pF	Cr=327 pF	340 pF
OLED 2	$R_{S2} = 150\ \Omega$	C2=13 pF	0	13 pF

Clearly, OLED2 which is fabricated with the second process offers improved high-speed features because of the removal of the parasitic capacitance induced by the photoresist of the first process. Nevertheless, one should wonder/consider if it is possible to obtain similar high-speed features with OLED1 by reducing the inactive area of the first process, and hence reducing C_R such that $C_2 = C_1 + C_R$ which means $C_R \sim 0$. In such a case, the inactive area is to be reduced to $S_{ITO} = 0$ mm^2. If such a reduction of the inactive area is implemented in OLED1 by the narrowing of the ITO strip then serial resistance will increase. Note that the capacitance C_R and the serial resistance are related by the geometry and a decrease of one causes an increase of the other because of he narrowing of the ITO stripe. Nevertheless, the process consisting in defining the OLED active area by the intersection of two perpendicular striped anodes and cathodes is to be preferred to the first one.

B. *OLED response*

The EL response in fig. 4.b and 5.b is in fact the OLED response (R(s) = H(s) . G(s)) composed by the electrical responses H(s) followed by the optical responses G(s). It means that the OLED response R(s) does not depends solely on OLED intrinsic parameters leading to G(s) but also depends on the electrical response. Rigorously, to access the optical pulse response G(s), R(s) is to be uncorrelated from H(s) which requires analytical expressions not available in the current study. However, in the special case in which H(s) would be similar to unity (H(s)~1), G(s) could be approximated by R(s). This happens if the electric system delivers an adiabatic answer for example if its time response is infinitely fast. Now, one should notice that experimental results of both devices exhibit electrical response times smaller than optical decay times ($\tau_{1E} < \tau_{1O}$ and $\tau_{2E} < \tau_{2O}$). In this context, and in first approximation the OLED response exhibits similar features similar than that of the optical response. Since the ($\tau_{2E} < \tau_{1E}$) the approximation is even more valid for OLED2 than for OLED1.

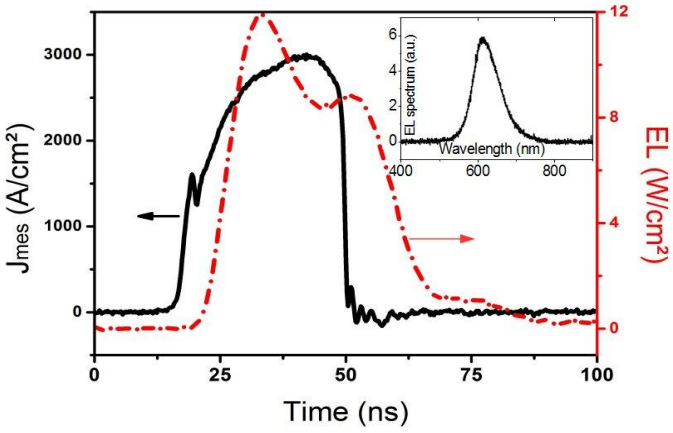

Fig. 6. Electric and optical response of OLED3 defined by electrode crossing

Note that the fact that $\tau_{1E} < \tau_{1O}$ and $\tau_{2E} < \tau_{2O}$ is an indication that both these fabrication processes allow the realization of high-speed organic optoelectronic devices, and authors believe this constitutes one definition for high-speed organic optoelectronics. Electrical response faster than the optical response allows the investigation of the physical and optical dynamics in organic optoelectronic devices under pulsed electrical excitation rather than under optical laser pulses as done so far. Indeed, because the electrical time response is smaller than the optical decay time, one can access under electrical excitation more easily to the intrinsic physical and optical properties of the OLED compounds.

C. *Optical response*

Although the optical decay time is just an aspect of the OLED impulse response and although there are other characteristics to be taken into account like OLED rise time and slew-rate, the authors focus the current optical response analysis on the optical decay time which plays an important role in the OLED dynamics. Indeed, the optical time decay is related to the onset of the polaronic absorption that reduces the singlet population and hence reduces the EL [11, 16].

The comparison of $\tau_{1O} = 12.1 \pm 0.5$ns and $\tau_{2O} = 9.8 \pm 0.2$ ns (from the optical waveforms fig. 4b and fig. 5b) shows that OLED2 decay time is faster than that of OLED1. As mentioned previously OLED2 provides a better approximation of the optical response because of a faster electrical response. This explain why OLED2 exhibits shorter decay time than OLED1 whereas the same organic compounds and the same thicknesses are used in both organic heterostrutures. In other words, OLED2 exhibiting faster electrical response than OLED1 ($\tau_{2E} < \tau_{1E}$) induces slightly faster optical response than OLED 1 ($\tau_{2O} < \tau_{1O}$) and hence reflects better the intrinsic physical and optical dynamics in the organic compounds.

VI. Break-down current density

To investigate the absolute maximum current density the study focused on OLED2 to proceed with the electric and optical measurements under higher voltage excitation. The maximum current without device failure was reached with a 30 ns pulse duration under excitation voltage increased up to 135 V. The corresponding current-density and EL waveforms are shown in Fig.6. The device exhibits a maximum current density of 3.0 kA/cm² and a maximum luminance of 12 W/cm². To the best of author's knowledge, this is the highest current density of an OLED obtained in the presence of the shortest electrical pulse reported so far. Authors believes even higher current densities can be achieved if the standard Organic heterostruture is to be improved with a PIN organic heterostructure [11]. Note that in the proposed structures, the fabrication of the OLED remains simpler and less expensive with photolithography instead of electron beam lithography [10].

VII. Conclusion

In this work, the OLED current density and electroluminescence time domain responses are studied numerically and experimentally at the nanosecond time scale. In section II a specific electrical model of µ-OLEDs in On-Off configuration has highlighted the role of the capacitances in the impulse response. In the device fabrication section, two types of µ-OLEDs are fabricated and compared in order to investigate experimentally the role of the capacitances of µ-OLED1 (113µm-diameter, S_1=0.01mm^2) defined by photolithography of an insulating photoresist, and µ-OLED2 (87×120µm^2, S_2=0.01mm^2) defined by electrode crossing. As shown in the characterization section, the second process allows better high-speed features with µ-OLED electrical time response as small as $\tau_{2E} = 2.1 \pm 0.6$ ns compared to $\tau_{1E} = 9.6 \pm 3.3$ ns obtained with a process based on photolithography. The fitting of the specific equivalent electric model based on the numerical analysis to the experimental results, demonstrates that the main limiting factor is indeed the device capacitance with $C_2 = 13$ pF in the second process, while it is $C_1 = 340$ pF with the first process. It is demonstrated that the larger capacitance is due to the photoresist used to limit the active area. Although an OLED as small as 1µm^2 can be fabricated with the first process, the higher capacitance resulting from the photoresist used to define the active area prevents from increasing further the OLED speed. Nevertheless, both processes provide optical time responses larger than the electrical one with $\tau_{1O} = 12.1 \pm 0.5$ ns $> \tau_{1E}$ and $\tau_{2O} = 9.8 \pm 0.2$ns $> \tau_{2E}$ which clearly classifies these organic optoelectronic devices as high-speed.

Finally, break-down current density as high as 3.0 kA/cm^2 and electroluminescence as high as 12 W/cm^2 are measured with the fastest µ-OLED.

As a perspective, authors consider the fabrication of smaller µ-OLEDs with faster response time and allowing even higher current density by reducing slightly further the ITO anode dimensions W_2 and L_2. Moreover, the difference between the electric and the optical time response indicates that it is possible to investigate the physical and optical dynamics without limitation of the electric time response. Authors believe this opens the possibility to investigate physical and optical dynamics in organic devices under pulsed-electrical rather than pulsed-laser excitation which is a step closer to the demonstration of the organic laser diode.

References

[1] J.-H. Jou, S. Kumar, A. Agrawal, T.-H. Li, and S. Sahoo, "Approaches for fabricating high efficiency organic light emitting diodes", J. Mater. Chem. C, vol. 3, no 13, p. 2974-3002, mars 2015.

[2] H. Sasabe and J. Kido, "Development of high performance OLEDs for general lighting", J. Mater. Chem. C, vol. 1, no 9, p. 1699-1707, Feb. 2013.

[3] B. Geffroy, P. le Roy, and C. Prat, "Organic light-emitting diode (OLED) technology: materials, devices and display technologies ", Polymer International, vol. 55, no 6, p. 572-582, juin 2006.

[4] Y. Cho and T. Daim, "OLED TV technology forecasting using technology mining and the Fisher-Pry diffusion model", Foresight, vol. 18, no 2, p. 117-137, avr. 2016.

[5] S. Chatterjee, S. Agarwal, A. Nath, and Kolkata, "Scope and Challenges in Light Fidelity(LiFi) Technology in Wireless Data Communication", International Journal of Innovative Research in Advanced Engineering (IJIRAE),ISSN: 2349, 2163, 6, Vol 2, (Jun 2015).

[6] P. Koos, T.Vorreau, P.Vallaitis, W.Dumon, R.Bogaerts, B.Baets, I.Esembeson, T.Biaggio, F.Michinobu, W. Diederich, Freude, andJ. Leuthold, "All-optical high-speed signal processing with silicon–organic hybrid slot waveguides", Nat Photon, vol. 3, nº 4, p. 216-219, avr. 2009.

[7] J. Clark and G. Lanzani, "Organic photonics for communications", Nature Photonics, vol. 4, no 7, p. 438-446, 2010.

[8] D. Calin, H. Claussen and H. Uzunalioglu, "On femto deployment architectures and macrocell offloading benefits in joint macro-femto deployments," in *IEEE Communications Magazine*, vol. 48, no. 1, pp. 26-32, January 2010.

[9] G. M. Akselrod, E. R. Young, K. W. Stone, A. Palatnik, V. Bulović, and Y. R. Tischler, « Reduced lasing threshold from organic dye microcavities », *Phys. Rev. B*, vol. 90, nº 3, p. 35209, juill. 2014.

[10] K. Hayashi, H. Nakanotani, M. Inoue, K. Yoshida, O. Mikhnenko, T.-Q. Nguyen, and C. Adachi, "Suppression faof roll-off characteristics of organic light-emitting diodes by narrowing current injection/transport area to 50 nm", Applied Physics Letters, vol. 106, no 9, p. 93301, mars 2015.

[11] D. Kasemann, R. Brückner, H. Fröb, and K. Leo, "Organic light-emitting diodes under high currents explored by transient electroluminescence on the nanosecond scale", Phys. Rev. B, vol. 84, no 11, p. 115208, 2011.

[12] B. Wei, M. Ichikawa, K. Furukawa, T. Koyama, and Y. Taniguchi, "High peak luminance of molecularly dye-doped organic light-emitting diodes under intense voltage pulses", Journal of Applied Physics, vol. 98, no 4, p. 044506-044506-5, august 2005.

[13] D. Buso, S. Bhosle, Y. Liu, M. Ternisien, C. Renaud and Y. Chen, "OLED Electrical Equivalent Device for Driver Topology Design," in *IEEE Transactions on Industry Applications*, vol. 50, no. 2, pp. 1459-1468, March-April 2014.

[14] V. C. Bender, T. B. Marchesan and J. M. Alonso, "Solid-State Lighting: A Concise Review of the State of the Art on LED and OLED Modeling," in *IEEE Industrial Electronics Magazine*, vol. 9, no. 2, pp. 6-16, June 2015.

[15] J. H. Sinsky, M. Duelk and A. Adamiecki, "High-speed electrical backplane transmission using duobinary signaling," in *IEEE Transactions on Microwave Theory and Techniques*, vol. 53, no. 1, pp. 152-160, Jan. 2005.

[16] T. Rabe, P. Görrn, M. Lehnhardt, M. Tilgner, T. Riedl, and W. Kowalsky, “Highly Sensitive Determination of the Polaron-Induced Optical Absorption of Organic Charge-Transport Materials”, Phys. Rev. Lett.